JOURNAL OF SPACECRAFT AND ROCKETS
Vol. 33, No. 3, May–June 1996

Experimental Investigation of Side-Jet Steering for Supersonic and Hypersonic Missiles

Julius Brandeis* and Jacob Gill*
RAFAEL, Ministry of Defense, Haifa 31021, Israel

An experimental investigation of the interaction between a side jet and the external flow is presented. The experiments were carried out in three different wind tunnels at supersonic and hypersonic Mach numbers ranging from 2 to 10. The model used in all the experiments consisted of a cylindrical body and various ogival nose sections, and had no lifting surfaces. The single sonic jet nozzle was located on the lee side of the cylindrical center body section with respect to a positive angle of attack. Several nozzle shapes and jet injection angles were examined. Forces and moments were measured directly in all the experiments, and surface pressure surveys were taken in some supersonic experiments. The results reveal a small jet force amplification at supersonic and hypersonic Mach numbers around zero angle of attack. Significant amplification because of positive angle of attack was noted at hypersonic speeds. The injection nozzle shape and vector angle can have a noticeable effect on the magnitude of the jet force amplification, especially at hypersonic speeds. In addition, the interaction gives rise to a significant pitching moment that may be utilized to produce an additional aerodynamic control force.

Nomenclature

C_m = pitch moment coefficient
F_i = interaction force, kgf
F_j = jet force at wind-on-conditions, kgf
F_{js} = jet force at wind-off conditions corrected for freestream static pressure conditions, kgf
K = jet amplification factor
M = freestream Mach number
$\dot{m}$ = jet mass flow rate, kg/s
P_{0t} = freestream stagnation pressure, kgf/cm^2
P_s = freestream static pressure, kgf/cm^2
Q = freestream dynamic pressure, kgf/cm^2
Re = Reynolds number
T_{0t} = freestream stagnation temperature, K
x = streamwise distance, m
α = angle of attack, deg

Introduction

SIDE jets have long been recognized as an effective means for maneuvering and controlling missiles and projectiles. When a jet is injected into the supersonic or hypersonic freestream, a complex flowfield is created, comprising various shock-wave patterns. The surface pressures induced by the interaction can, under certain conditions, lead to an increase in the direct force control. Such force amplification has been reported in a number of prior publications.[1–4] This paper studies experimentally the ways of maximizing the amplification effect, to obtain larger control forces and moments. The wind-tunnel experiments were conducted in various facilities, for supersonic and hypersonic Mach numbers.

The typical flow topology and surface pressure pattern for such jet interaction are shown in Fig. 1. The jet issuing into the supersonic or hypersonic freestream acts as an obstacle to the flow and produces a strong shock wave, called the jet bow shock. The disturbance propagates upstream through the boundary layer, causing a wedgelike region of separated flow ahead of the jet, with its separation shock and elevated surface pressure. The downstream surface pressures are generally lower than ambient in supersonic flow, but are reported to be higher than ambient at hypersonic speed.[2]

Presented as Paper 95-0316 at the AIAA 33rd Aerospace Sciences Meeting and Exhibit, Reno, NV, Jan. 9–12, 1995; received Jan. 23, 1995; revision received May 22, 1995; accepted for publication June 3, 1995.

*Research Engineer, Aeronautical Systems Department, P.O. Box 2250. Member AIAA.

The interaction amplification factor K is defined here as the sum of the interaction force and the jet thrust, divided by the jet thrust at wind-off conditions corrected for the freestream static pressure conditions, as follows:

$$K = \frac{F_i + F_j}{F_{js}}$$

The amplification factor can be increased by mounting the injection nozzle at the aft end of the body, thereby eliminating the downstream low-pressure region.[3] The bow shock tends to wrap around the body, producing high pressure on the underside, and hence reducing the jet amplification factor.[5,6] In this way the three-dimensional interaction differs from the planar case.[1,2,4]

Another effect noted in this work, which may be very useful for vehicle control, is the induced moment resulting from the upstream and the downstream interaction. As noted, the upstream overpressure and the downstream underpressure regions produce a nose-down moment couple about the injection location. The resulting angle of attack gives rise to an aerodynamic force that acts in the same direction as the direct thrust force and can serve to increment

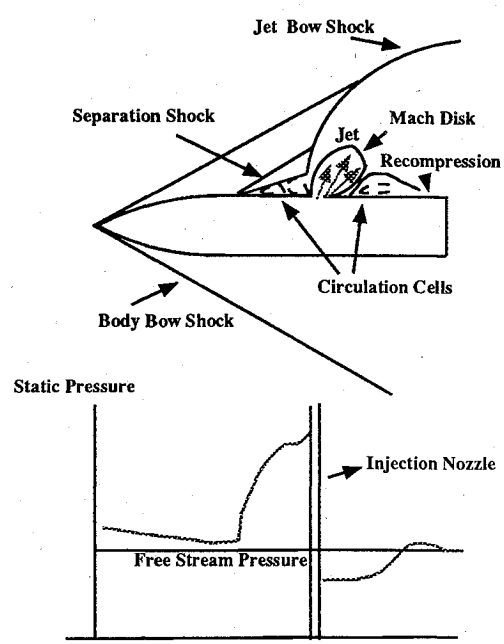

Fig. 1 Jet-interaction flowfield and surface pressures.

further the control force. If a specific body attitude is to be maintained, then these moment-induced effects can be undesirable.

Experimental Setup and Procedure

Description of the Wind-Tunnel Model

A versatile wind-tunnel model was built to allow force and moment measurement, as well as a surface pressure survey. The gas used in the jet was atmospheric air supplied through the balance. The model admits various forebody shapes, as seen in Fig. 2, as well as various jet nozzles of different sizes and shapes: circular, rectangular, multiple or vectored (see Fig. 3 and Table 1). All nozzles discussed were designed to achieve sonic flow at the exit. The test model is composed of interchangeable forebody and afterbody sections and the main central section containing the balance mounting point, the jet plenum (stagnation chamber), and the mounting for the interchangeable jet-nozzle plates. The central section is the heart of the model and is used as the mounting piece for the fore and aft segments. When fully assembled and with the nozzle closed, the central section is a pressure vessel tested to withstand hydrostatic pressures of up to 70 atm.

One ogival forebody and one cylindrical afterbody were instrumented with static pressure taps. A total of about 100 pressure taps were used. Pressure measurements were not performed in the hypersonic tests, because the static pressures on the model surface were very low. The reference diameter of the model is 50 mm (cylindrical section diameter), and the total length is 315 mm for the standard model including ogival forebody of $1/d = 4$. The nozzle exit is located at $x = 225$ mm from the nose tip. Use of different components resulted in different overall model length.

Table 1 Various nozzles

Nozzle[a]	Description	Size, mm	Vector angle, deg
1	Rectangular slit	9 × 2.2	0
2	Rectangular slit	13.5 × 1.5	0
		20 × 2.5[b]	0
3	Rectangular slit	13.5 × 1.5	30
		20 × 2.5[b]	45
4	Circular	5	0
5	Circular	8	0
			45[b]
6	Twin circular	5.6 each	0

[a]See Fig. 1. [b]Shape not shown in Fig. 1.

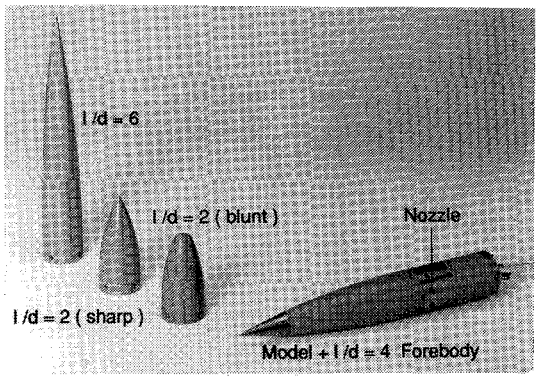

Fig. 2 Model and forebodies.

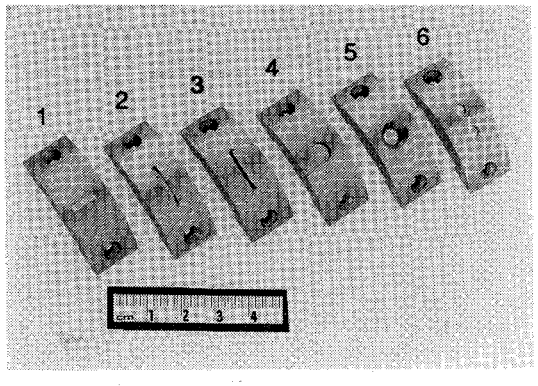

Fig. 3 Various nozzles.

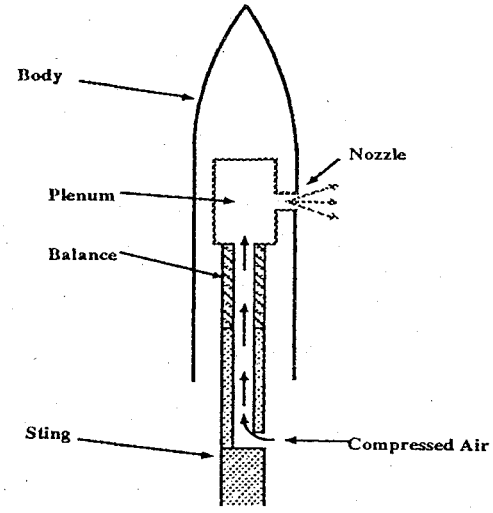

Fig. 4 Schematic view of body and balance setup.

Balance

The balance and the sting were specially designed for these experiments at the Technion balance shop. The four-component balance measures the normal and side forces and the pitching and yawing moments only (no drag and roll components). The injectant gas is atmospheric air at reservoir temperature and is fed by a coaxial tube through the sting–balance into the plenum chamber within the model. The balance design and model mounting method were such as to assure that gas feed did not induce any disturbance that could affect the measurements. A schematic view of the balance and the model setup is shown in Fig. 4.

Experimental Procedure

Experiments were divided into two distinct series. In the first series, forces and moments were measured using the components of the model not instrumented for the pressure measurements. The second part was dedicated to pressure measurements.

The usual sequence of the force experiments was as follows:

1) Calibration experiment, measuring the jet thrust force with the specific nozzle at specified stagnation pressure (no wind in the tunnel). This thrust force can then be corrected for the actual freestream static pressure conditions prevailing in the actual wind on experiment.

2) Base experiment, measuring the forces and moments of a configuration at the desired Mach number, but without activating the jet. The jet nozzle was replaced with a cover plate in such experiments, to achieve a smooth model surface. Full angle-of-attack sweep is carried out.

3) Reference experiment with jet injection, at the desired Mach number and with the full angle-of-attack sweep.

Each experiment was carried out at a designated Mach number with the side jet activated at a selected stagnation pressure. At some Mach numbers, tests were done with various stagnation pressures. the mass flow rate was determined from a calibrated nozzle in the supply line. Pressures were measured in the jet stagnation chamber and also in a nozzle within the gas supply line to ascertain that the pressure measured in the chamber was indeed the stagnation pressure.

For the surface pressure survey experiments, no force or moment data were recorded, because such force measurements can be influenced by the presence of multiple steel pressure tubes within the model and can be unreliable. The balance was, however, used in those experiments to determine the sting bending (which causes a deviation in the angle of attack) resulting from loads, thus allowing

the determination of the actual angle of attack. The pressure measurements were made via three Scanivalves, with some locations sampled twice for a check. The pressure measurements were made at discrete angles of attack and not in the sweep procedure used in the force experiments.

Experimental Results

The experiments were carried out at three different wind tunnels to achieve the desired Mach number range of 2–10. The consequence of testing at such a wide range of Mach numbers is therefore that the experiments were carried out at different reference static pressures, densities, and temperatures in the test section. Equivalent experiments that were carried out in the Technion supersonic wind tunnel and in the Israel Aircraft Industries (IAI) supersonic tunnel, at Mach 3.3, showed excellent agreement with the measured data. The effective altitude in the test section of these tunnels is presented in Fig. 5. The test conditions and the flow regimes in the various facilities are summarized in Table 2.

Configurational Effects (Supersonic Speeds)

The base model configuration, comprising an ogival nose of $1/d = 4$, centerbody of $1/d \approx 1$, and cylindrical aft section of $1/d \approx 1$, was tested at the full Mach number range. However, at the supersonic Mach numbers 2.0 and 3.3, several other forebodies with $1/d$ ratio of 2, 4, and 6 and different nose tip shapes (sharp and blunt) as shown in Fig. 2, were also tested. The measured results show that the forebody shape and length have only a very small influence on the jet-interaction force and on the induced pitching moment created by the pressure region around the nozzle (to be discussed). The flows for $1/d = 2$ blunt and sharp nose configurations are compared in the schlieren photographs in Figs. 6a and 6b. For both configurations, a single, 8-mm-diam sonic nozzle was used. The mass flow rate was 0.50 kg/s at the chamber pressure of 55 atm. Note that two shock waves are discernible on the bottom surface of the model. The forward one may be associated with the jet separation and bow shock, and the downstream one (almost at the base of the model) may be due to the recompression shock downstream of the jet. There is an indication of boundary-layer separation downstream of the first shock.

Figure 7a shows the flowfield for the standard configuration having the $1/d = 4$ ogival nose section and a cylindrical $1/d \approx 1$ aft section. The freestream Mach number is 3.3. The jet nozzle and flow properties are similar to the case previously discussed. The shock

Table 2 Flow conditions for the wind tunnels used

Mach no.	P_{0t}, kg/cm^2	P_s, kg/cm^2	Q, kg/cm^2	T_{0t}, K	Re, 10^6 m^{-1}
2.0[a]	3.8	0.48	1.35	279	50
3.3[a]	11.5	0.19	1.45	271	78
3.3[b]	6.54	0.114	0.87	312	37
4.8[b]	16.9	0.04	0.65	310	46
8.0[c]	26.7	0.00274	0.123	736	5.9
10.0[c]	31.3	0.00074	0.052	754	3.95

[a]Technion supersonic wind tunnel. [b]IAI supersonic wind tunnel.
[c]IAI hyersonic wind tunnel.

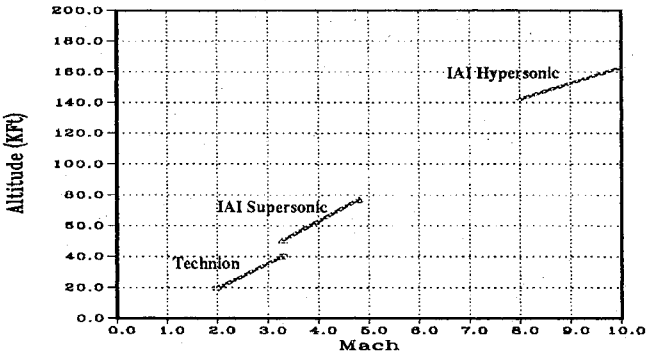

Fig. 5 Flow conditions for the wind tunnels used.

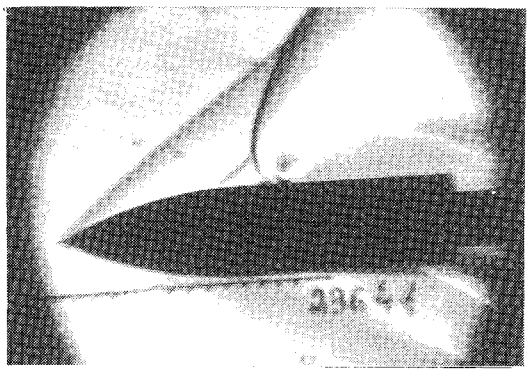

Fig. 6a Sharp $1/d = 2$ nose, $M = 2$, 8-mm circular nozzle, $\dot{m} = 0.5$ kg/s.

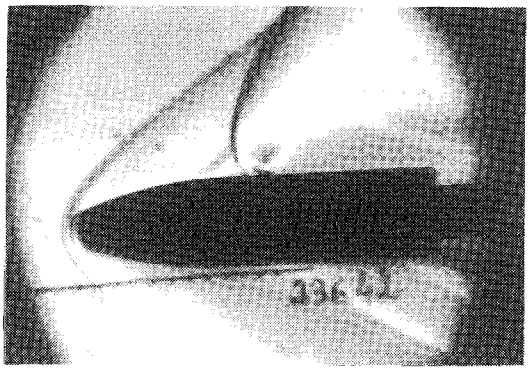

Fig. 6b Blunt $1/d = 2$ nose, $M = 2$, 8-mm circular nozzle, $\dot{m} = 0.5$ kg/s.

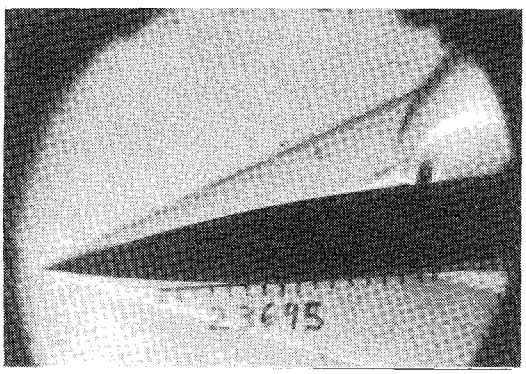

Fig. 7a Sharp $1/d = 4$ nose, $M = 3.3$, 8-mm circular nozzle, $\dot{m} = 0.55$ kg/s.

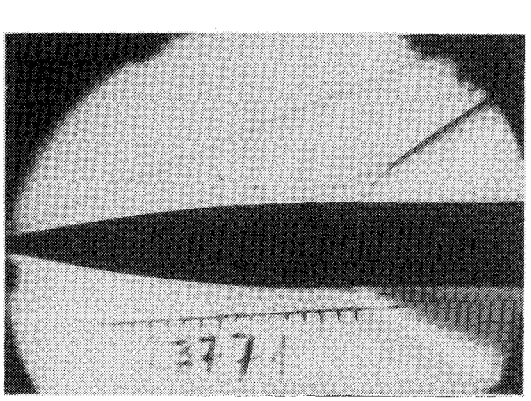

Fig. 7b Model as in Fig. 7a, rotated 90 deg, with 4-deg sideslip angle.

at the underside is visible, as is some boundary-layer separation. A flow visualization for this case looking from the underside of the model (i.e., with the model rolled 90 deg around its axis) is presented in Fig. 7b. The model is shown at a sideslip angle of 4 deg. Note the significant lateral penetration of the separation shock and the bow shock. The extent to which the jet shock wave wraps around the body cannot be judged from these schlieren images.

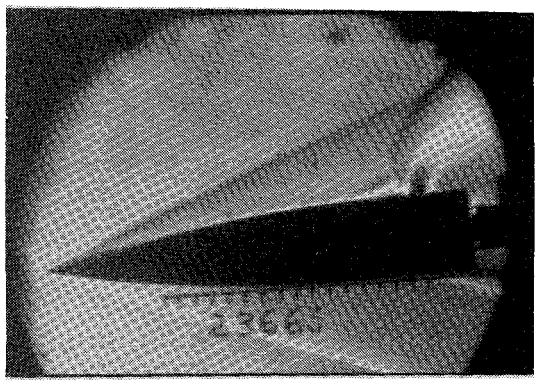

Fig. 8 Sharp $1/d = 4$ nose, no afterbody, $M = 3.3$, 8-mm circular nozzle, $\dot{m} = 0.53$ kg/s.

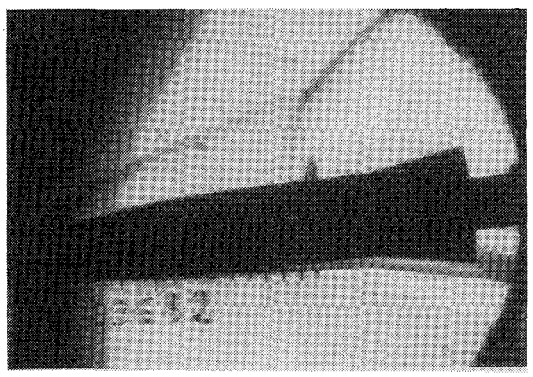

Fig. 9 Sharp $1/d = 4$ nose, flared afterbody, $M = 3.3$, 8-mm circular nozzle, $\dot{m} = 0.53$ kg/s.

Tests were carried out at $M = 3.3$ with the cylindrical aft section of the model removed, to investigate the effect of the downstream region on the interaction, as shown in Fig. 8. Note that not all of the downstream surface has been eliminated, since the nozzle was mounted on the forward portion of the center body. The same jet parameters reported earlier were used here. The reduction in the surface area within the downstream interaction region caused a 10% net force amplification, confirming that the downstream region gives a significant negative contribution to the interaction force. At the same time, the induced-moment coefficient was correspondingly reduced to half its value with the aft section present. The strong influence of the jet nozzle axial location has been noted by Gillman,[3] who reports 20% increase in the control force at $M = 2.0$ with exit nozzle location at the very base of the model, compared to the midbody location.

A 10-deg flare was mounted over the cylindrical aft section downstream of the nozzle, and the configuration was tested at $M = 3.3$ (again, the same jet parameters). The schlieren photograph of one such test in Fig. 9 shows the jet flow structure and its interaction with the external flow. The flow on the underside is especially clear, with the shock-induced boundary-layer separation that fails to attach to the flare. The results, for two different flare locations, show a 12% decrease in normal force, whereas the pitching moment was much larger (depending on flare location) than that obtained with just the cylindrical aft section. These results again confirm the importance of the downstream region, including the low pressures in the wake of the jet and the effects of the jet bow shock wave on the bottom surface of the model.

Effect of Angle of Attack and Nozzle Geometry on Force Amplification

The measured force amplification at zero angle of attack remained small even at hypersonic Mach numbers. A significant increase in the force amplification at positive angles of attack was, however, measured for all the experiments carried out at hypersonic Mach numbers. Such influence is shown in Figs. 10–12, in which the jet thrust force and the jet interaction force, together with the calculated

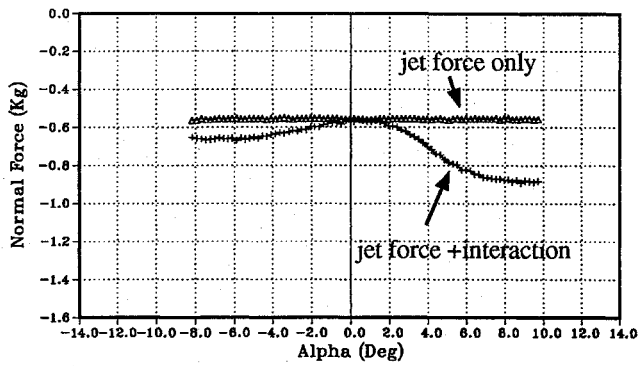

Fig. 10a Normal-force variation at $M = 8$, circular upright nozzle, $\dot{m} = 0.011$ kg/s.

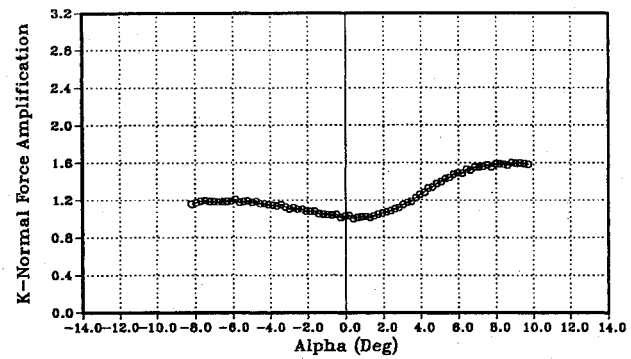

Fig. 10b Amplification-factor variation at $M = 8$, circular upright nozzle, $\dot{m} = 0.011$ kg/s.

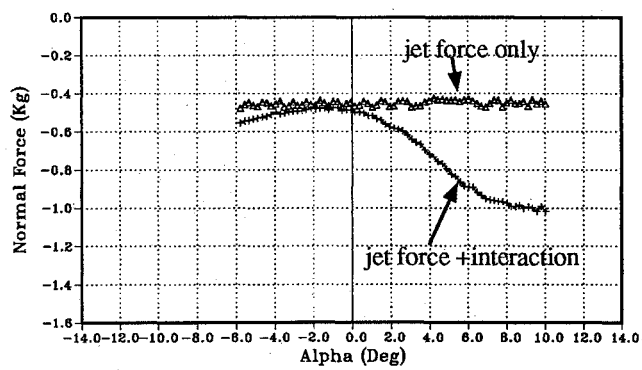

Fig. 11a Normal-force variation at $M = 8$, rectangular nozzle inclined 30 deg upstream, $\dot{m} = 0.011$ kg/s.

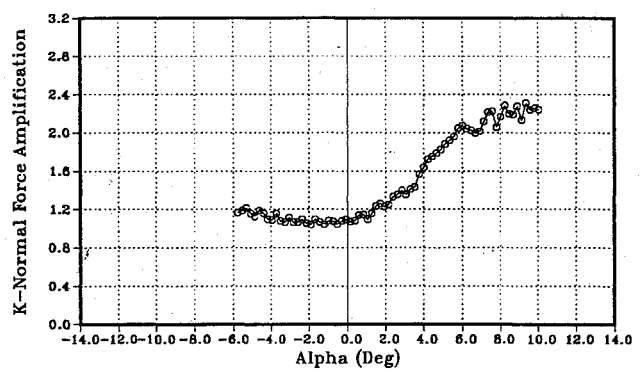

Fig. 11b Amplification-factor variation at $M = 8$, rectangular nozzle inclined 30 deg upstream, $\dot{m} = 0.011$ kg/s.

net amplification factor, are presented as functions of the angle of attack. The results presented are for three different sonic nozzles: a circular 5-mm-diam nozzle directed upright (90 deg) shown in Figs. 10a and 10b, a rectangular 13.5 × 1.5 mm nozzle vectored 30 deg upstream (Figs. 11a and 11b), and the same rectangular nozzle facing 30 deg downstream (Figs. 12a and 12b), all at $M = 8$. The jet nozzle was located in the upper surface of the model, as

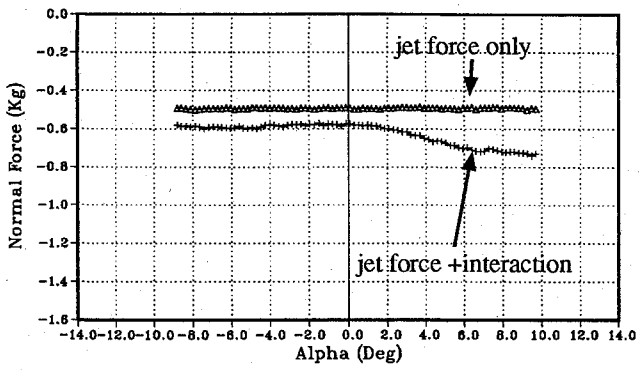

Fig. 12a Normal-force variation at $M = 8$, rectangular nozzle inclined 30 deg downstream, $\dot{m} = 0.011$ kg/s.

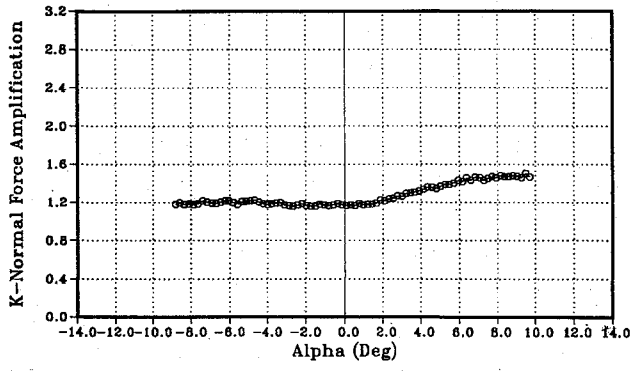

Fig. 12b Amplification-factor variation at $M = 8$, rectangular nozzle inclined 30 deg downstream, $\dot{m} = 0.011$ kg/s.

mounted in the tunnel, and therefore the thrust force presented is in the negative (downward) direction. The datum thrust of the two inclined rectangular nozzles is smaller than the datum thrust for the normal circular nozzle. Part of the difference is a result of the nozzle inclination angle, and part is a result of the geometrical effect.

A major magnification in the interaction force is noticed for positive angle of attack, reaching a maximum for $\alpha > 6$ deg. Negligible amplification is present near zero, and for most cases there is some increase in the amplification at negative angles of attack. The reason for this phenomenon is not quite clear, but it is probably related to the changes in the flowfield in the downstream region and to the change in the shock pattern relative to the body, especially along the lower surface. For positive angles of attack Fig. 11 shows that the rectangular, forward-directed nozzle gives rise to the largest amplification factors, reaching the value of 2.2 at 7-deg angle of attack. This value is significantly larger than the amplification factors obtained for the other nozzles. The corresponding total control force, however, shows a smaller advantage because of the smaller datum thrust of the forward-pointing rectangular nozzle.

As noted, large amplification factors were obtained for all cases at positive angles of attack. At very small angles of attack, the largest interactive force magnification is achieved with the backward directed injection, as can be seen by comparing the cases presented in Figs. 10–12. Note that the total control force for this case was not greater than that for the normal circular nozzle (Fig. 10). The forward-vectored nozzle, although causing the longest upstream disturbance (as will be shown in the surface pressure plots), results in the smallest relative force amplification, and smallest total control force at $\alpha \approx 0$ deg. These results are consistent with the findings at supersonic Mach numbers. The rectangular nozzles, facing the flow with the long dimension, resulted in marginally higher amplification factors than noted for the equivalent area circular nozzle, and the slit nozzle with the narrow dimension facing the flow achieved the lowest amplification.

Effect of Mach Number on Force Amplification

The normal-force amplification factor K is plotted as a function of Mach number for the circular nozzle in Fig. 13, and for the

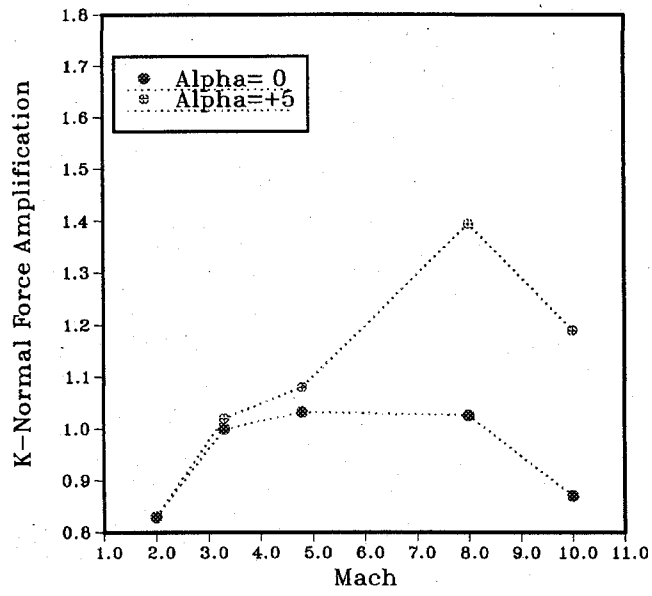

Fig. 13 Jet force amplification for circular upright nozzle of 5-mm diam.

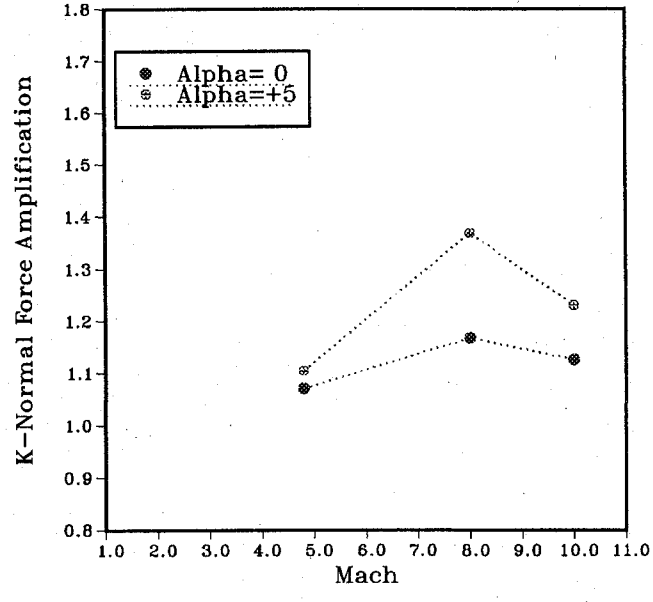

Fig. 14 Jet force amplification for rectangular 13.5 × 1.5 mm nozzle inclined 30 deg downstream.

rectangular (slit) nozzles vectored 30 deg downstream in Fig. 14. These results were obtained using various flow conditions, but for the same standard model configuration. The jet force amplification at angle of attack $\alpha \approx 0$ deg in the supersonic region was quite small, as shown in Figs. 13 and 14. At $M = 2.0$ there was even a large (17%) decrease in jet control force due to the interaction. At $M = 3.3$, 0–3% force amplifications were measured, and at $M = 4.8$, 4–8%. A noticeable increase in the jet force amplification was achieved at Mach number $M = 8$ (up to 18% amplification with a rectangular nozzle, and about 3% with a circular nozzle at $\alpha \approx 0$ deg. However, much smaller values of the amplification are noticed at Mach number 10 (up to 13% decrease for the circular nozzle at $\alpha \approx 0$ deg. The best jet amplification results were achieved with a rectangular nozzle at $M = 8$, vectored downstream by 30 deg, at $\alpha \approx 0$ deg. The peak K values in Figs. 13 and 14 occur at $M = 8$. The drop in K at $M = 10$ is not understood, and it contradicts the findings reported in literature. Note that jet injection at $M = 10$ caused a significant disturbance in the tunnel flow conditions, and therefore measurements at this speed may be subject to error. Flow laminarization because of the decrease in Reynolds number relative to the $M = 8$ case may also be a possible explanation of the discrepancy.

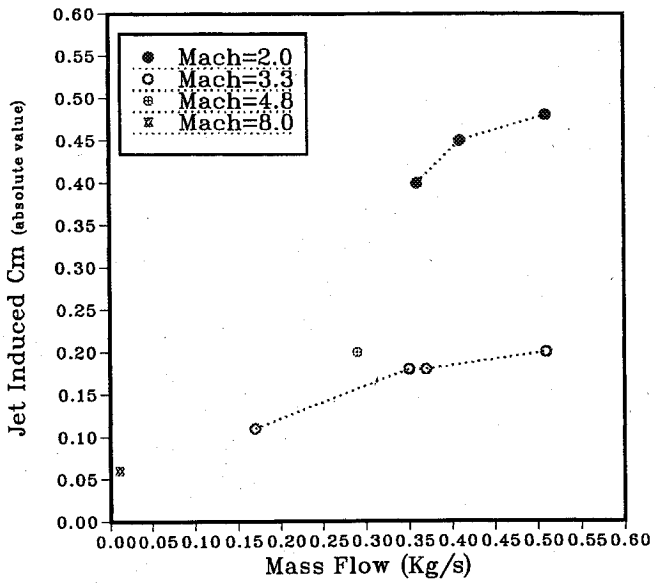

Fig. 15 Jet-interaction-induced pitching-moment coefficient.

Jet-Induced Moments

In addition to the direct force amplification, the experimental results also indicate the presence of significant interaction-induced pitching moments because of the force couple derived from the pressure distribution around the jet nozzle. The aerodynamic lateral force arising from the attitude of the body can effectively increase the control force. The measured pitching moments were calculated for the configurations presented at Mach numbers of 2 and 3.3, to result in trim angles of attack ranging between 1 and 10 deg, depending on the configuration. The center of moments was taken at the nozzle location.

The absolute value of the induced pitching-moment coefficient as a function of the mass flow rate is shown in Fig. 15. Data for four different Mach numbers are plotted, all for circular nozzles. For Mach numbers 2 and 3.3, there is a definite increase of the pitching moment with increasing mass flow rate. At the remaining Mach numbers, the data were insufficient to draw any conclusions. Attempts to unify the data for all Mach numbers by plotting the product of C_m and the jet-to-tunnel momentum ratio did not give meaningful results.

The induced-moment effect around the nozzle may be an attractive and practical additional factor for controlling high-speed missiles and projectiles when the jet is applied at or forward of the center of gravity. For application of the jet at the rear of the configuration, used for pitch control, the interaction-induced pitching moment counteracts the effect of the jet, and should be minimized. In some cases of divert-jet application at the center of gravity, when maintaining the body orientation angle is important, the interaction moment may also be a parasitic effect.

Surface Pressure Results

The surface pressure experiments measured the pressures within the regions of jet interaction to explain some of the results obtained with force measurements. The experiments in this series were all performed at Mach number 3.3 in the Technion tunnel, and used the specific model configuration: $1/d = 4$ ogival sharp nose and $1/d = 3$ cylindrical afterbody. The main parameters varied were the nozzle geometry and flow rate (which depends on the jet stagnation pressure and nozzle exit area). The pressure experiments paralleled closely the force measurement experiments. The pressure results were plotted for sections (cuts) containing multiple pressure measurement locations, both in the axial directions and in the cross planes upstream and downstream of the jet location. No pressure taps were located on the underside section of the model. The axial surface pressure plots in Figs. 16 and 17 illustrate the effect on the surface pressures of various nozzle shapes and injection angles, respectively, at zero angle of attack. The data are presented along the meridian line containing the nozzle. Note especially the large

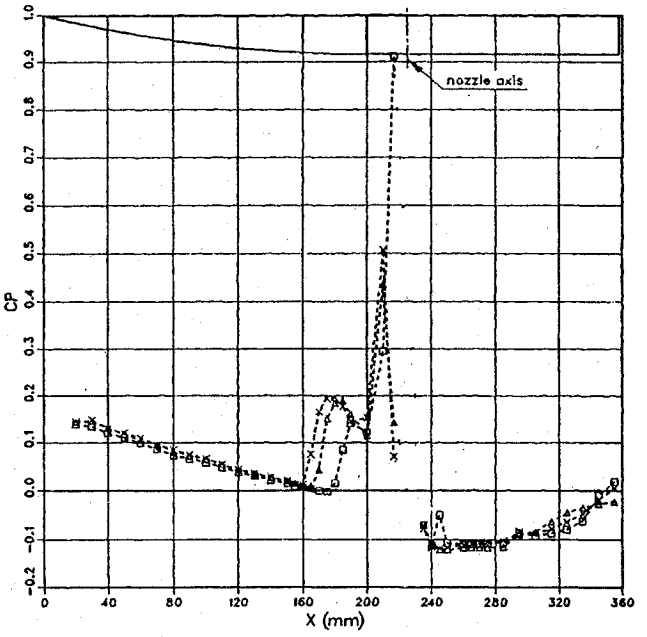

Fig. 16 Effect of nozzle geometry on surface pressures for normal injection: □, 8 mm circular nozzle; △, twin 5.5 mm nozzle; and ×, rectangular 20 × 2.5 mm nozzle.

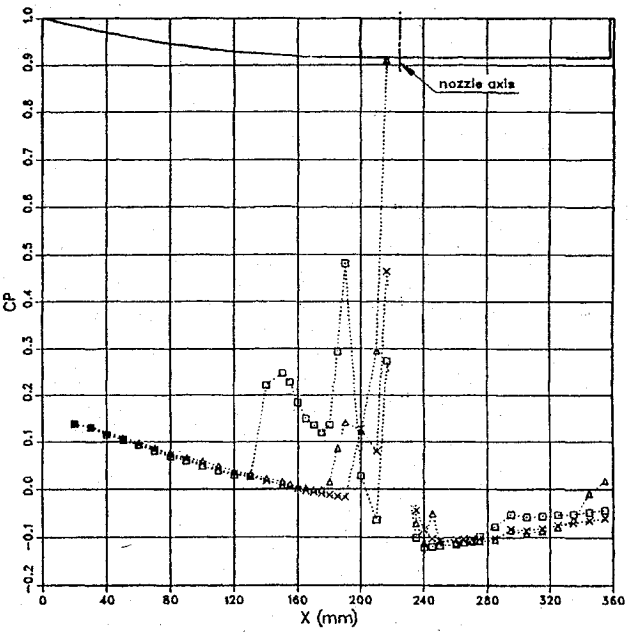

Fig. 17 Effect of injection angle on surface pressures for 8-mm-diam circular nozzle: □, 45 deg upstream; △, normal; and ×, 45 deg downstream.

changes in the length of the upstream separated region, because of the jet vector angle, in Fig. 17. Figure 16 shows that the nozzles producing a jet of large frontal area facing the external flow (the rectangular slit nozzle) produce the largest upstream separation. The nozzle geometry was noted to affect the size of the upstream separation region roughly to the same extent as the variation in the jet stagnation pressure (comparison not shown). Note that neither the nozzle geometry, or the jet vector angle affected the downstream pressures significantly. The large pressure spike located just upstream of the nozzle probably indicates the location of the jet bow shock.

Conclusions

The jets, together with the associated force and moment interaction effects, can be a very attractive and practical means for controlling high-speed missiles and projectiles within a dense atmosphere.

The interaction induces a high-pressure region upstream and a low-pressure region downstream of the jet. The upstream region increases the control force, and the downstream region decreases it. The effect of the downstream region on the jet force amplification and on the jet induced moment proved to be of major importance. The strong shock upstream of the jet appears to wrap around the projectile, and exerts a force in the direction opposite to the jet thrust on the downstream part of the body. This downstream force is configuration-dependent.

Very significant amplification was obtained at positive angles of attack for hypersonic Mach numbers. At $\alpha \approx 0$ deg the maximum value of jet amplification (18%) was achieved for the case of a rectangular nozzle inclined with the flow. The force results were sensitive to the nozzle geometry, with best results obtained for nozzles that produce a jet with large frontal area relative to freestream. This can be explained by the jet interaction effects, as the inclined rectangular nozzles have a smaller datum thrust than the equivalent normal circular nozzle. The force results were insensitive to forebody shape and size.

Flared afterbodies caused a decrease in normal force. By removing the cylindrical afterbody a 10% force magnification was obtained because a large portion of the surface over which the low pressure acts was removed. The presence of rear-mounted flare increases the pitching moment because the downstream jet interaction is stronger than for a cylindrical afterbody.

The contribution of the pitching-moment-induced force, relative to the direct thrust, was found to be inversely proportional to the mass flow rate. (Small mass, large aerodynamic contribution.) It depends on various configuration-dependent factors, such as the relative location of the centers of pressure and gravity and the jet axis.

Acknowledgment

This work was funded jointly by RAFAEL and Defense Department Research and Development–Mafat.

References

[1]Spaid, F. W., and Zukoski, E. E., "A Study of Interaction of Gaseous Jets from Transverse Slots with Supersonic External Flows," *AIAA Journal*, Vol. 6, No. 2, 1968, pp. 205–212.

[2]Spaid, F. W., "Two-Dimensional Jet Interaction Studies at Large Values of Reynolds Numbers," *AIAA Journal*, Vol. 13, No. 11, 1975, pp. 1430–1434.

[3]Gillman, B. G., "Control Jet Investigation," *Journal of Spacecraft and Rockets*, Vol. 8, No. 4, 1971, pp. 334–339.

[4]Brandeis, J., "Numerical Study of Jet Interaction at Super and Hypersonic Speeds for Flight Vehicle Control," *Proceedings, 18th Congress, International Council of the Aeronautical Sciences* (Beijing, China), International Council of the Aeronautical Sciences/AIAA, Washington, DC, 1992 (ICAS Paper 92-4-9.1).

[5]Hsieh, T., and Wardlaw, A. B., Jr., "Numerical Simulation of Cross Jet in Hypersonic Flow over a Biconic Body," AIAA Paper 94-0165, Jan. 1994.

[6]Yeneriz, M. A., Davis, J. S., Cooper, G. K., and Harvey, D. W., "Comparison of Calculation and Experiment for a Lateral Jet from a Hypersonic Cross-Flow," AIAA Paper 89-2548, July 1989.

R. M. Cummings
Associate Editor